

Negative transit time in non-tunneling electron transmission through graphene multilayers

E. E. Krasovskii^{1,2,3} and R.O. Kuzian^{2,4}

¹*Universidad del País Vasco/Euskal Herriko Unibertsitatea,
20080 Donostia/San Sebastián, Basque Country, Spain*

²*Donostia International Physics Center (DIPC),
20018 Donostia/San Sebastián, Basque Country, Spain*

³*IKERBASQUE, Basque Foundation for Science, 48013 Bilbao, Basque Country, Spain*

⁴*Institute for Problems of Materials Science NASU, Krzhizhanovskogo 3, 03180 Kiev, Ukraine*

Attosecond dynamics of electron transmission through atomically-thin crystalline films is studied with an *ab initio* scattering theory. The temporal character of the electron propagation through graphene multilayers is traced to the band structure of bulk graphite: In the forbidden gaps the wave packet transit time τ_T saturates with thickness and in the allowed bands τ_T oscillates following transmission resonances. Hitherto unknown negative transit time due to in-plane scattering is discovered in monolayers of graphene, h-BN, and oxygen. Moreover, Wigner time delay is found to diverge at the scattering resonances caused by the emergence of secondary diffracted beams. This offers a way to manipulate the propagation timing of the wave packet without sacrificing the transmitted intensity. The spatial reshaping of the wave packet at the resonances may help elucidate details of the streaking by an inhomogeneous field at the surface.

The question of how long does it take for a quantum particle to transit from one point to another arises in various physical contexts, including nanotransport, photonics, and photoelectron spectroscopy. There, one encounters paradoxical phenomena, such as the Hartman effect [1]—a fundamental aspect of wave propagation in a totally reflecting medium whereby the traversal time of a wave packet across a finite slab is independent of the slab thickness for sufficiently thick slabs. The implied unlimited velocities inspired a lively theoretical discussion [2–6] and triggered much experimental effort in optics [7–12] strong-field ionization [13–15], and atomic tunneling [16]. The superluminality paradox has called for a refined understanding of the notion of propagation velocity and a rigorous definition of the transit time [2–4]. However, over the many decades the discussion has been limited to tunneling under a barrier, while temporal paradoxes in classically allowed transmission have not been addressed.

The progress in attosecond photoelectron spectroscopy of crystals [17–24] has given new prominence to the question of how fast a quantum particle traverses a microscopic distance. The measured phase shifts of the streaking spectrograms [25] are commonly interpreted in terms of the escape time of photoelectrons originating at a depth of the order of the mean free path [17]. While there have been attempts to understand the results in terms of group velocity, this is not strictly justified and completely fails in a band gap.

A rigorous way to proceed is to draw on the Wigner time delay $\Delta\tau$, which is defined as the difference in the time of arrival of a free particle and a scattered one in a region far from the scatterer, see Fig. 1(d). It can be obtained from the stationary states of the system as the energy derivative of the scattering phase [26–28]. Here, we apply the phase-time formalism to a tunneling-free propagation in experimentally accessible graphene multilayers. $\Delta\tau$ is calculated with a state-of-the-art band struc-

ture accuracy using the augmented-plane-waves based scattering theory [29]. We obtain realistic values for the saturated transit time in the gaps and investigate the temporal characteristics of transmission (T) resonances. Most important, we reveal the essential role of the lateral scattering, which is inevitably present in realistic three-dimensional (3D) crystals, but has been completely ignored in previous theoretical (exclusively 1D) studies. Electron scattering from the monolayers of graphene and hexagonal boron nitride (h-BN) allows to separate out the lateral scattering and reveals a striking effect: at the T -resonance due to the emergence of the secondary diffraction beams the Wigner delay acquires large negative values, which results in a negative transit time.

This effect can be measured in a laser streaking experiment: A subfemtosecond XUV pulse excites a localized state just below the surface, Fig. 1(a), and the outgoing photoelectron is scattered by the surface overlayer, Fig. 1(b), and further exposed in vacuum to the laser streaking field synchronized with the XUV pulse, Fig. 1(c). The arrival time is then inferred from the momentum transferred from the laser field to the electron [17–24]. Based on the time delay $\Delta\tau$, Hartman [1] introduced so-called transmission time τ_T , which implies that the distance l traveled by a wave packet can be divided into scattering region d and free-motion region $l-d$, and that the time to traverse the full length l (arrival time [30, 31]) equals the sum of the two partial times. Although not rigorous [32, 33], this procedure is widely applied in analyzing the times of photoemission from surfaces or strong-field ionization of atoms. Here, we ascribe by convention the width $d = na$ to an n ML slab, where a is the interlayer spacing. Then, $\tau_T = \Delta\tau + d/v_0$.

Let us consider an infinitely spectrally narrow wave packet normally incident on a crystalline film located between z_L and z_R (outside this interval the electron potential equals zero), see Fig. 1(b). The scattering wave

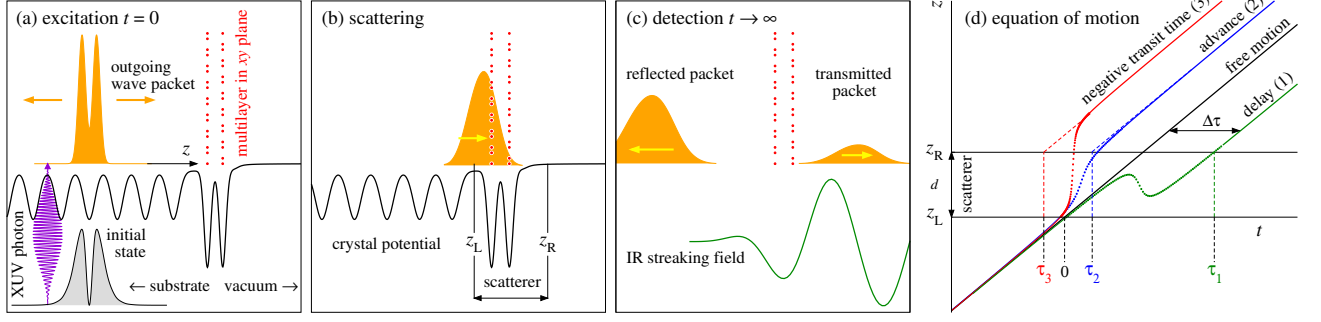


FIG. 1. (a)–(c) Scattering configuration and a sketch of a relevant experiment. Excited (a), incident (b), reflected and transmitted (c) wave packets are shown by orange shading. (d) Schematic equations of motion $z(t)$ of the incident and transmitted packets for positive (case 1) and negative (2 and 3) time delay $\Delta\tau$. Straight solid lines show the asymptotic free motion, and dots symbolically indicate the region where $z(t)$ is undefined. The transit time is defined as the extrapolation of the $t \rightarrow \infty$ line to the right border of the scatterer, $z = z_R$. Time delay (1) is typical of transmission resonances, see Fig. 3. Time advance with a positive transit time (2) is realized in the Hartman effect. Case 3 is a new finding of the present work.

function satisfies the Schrödinger equation $\hat{H}\Psi = E\Psi$ with initial conditions implying the presence of the incident and reflected wave(s) in the left half-space, $z < z_L$, and transmitted wave(s) in the right half-space, $z > z_R$:

$$\Psi = \begin{cases} e^{ik_0z} + \sum_{\mathbf{g}} r_{\mathbf{g}} e^{i[-k_{\mathbf{g}}(z-z_L) + \mathbf{g}\mathbf{r}_{\parallel}]}, & z \leq z_L, \\ \sum_{\mathbf{g}} t_{\mathbf{g}} e^{i[+k_{\mathbf{g}}(z-z_R) + \mathbf{g}\mathbf{r}_{\parallel}]}, & z \geq z_R, \end{cases} \quad (1)$$

where \mathbf{r}_{\parallel} is the surface parallel radius vector and \mathbf{g} are 2D reciprocal lattice vectors. The incident wave vector is $k_0 = \sqrt{2mE}/\hbar$, and z -projections of the wave vectors of the secondary beams, $\mathbf{g} \neq 0$, are $k_{\mathbf{g}} = \sqrt{2mE/\hbar^2 - |\mathbf{g}|^2}$. The scattering state Ψ is calculated with the *ab initio* embedding method in terms of augmented plane waves [29], see Appendix A. Equation (1) introduces the transmission and reflection coefficients: $t_{\mathbf{g}} = |t_{\mathbf{g}}| \exp(i\xi_{\mathbf{g}}^t)$ and $r_{\mathbf{g}} = |r_{\mathbf{g}}| \exp(i\xi_{\mathbf{g}}^r)$. The scattering phase shift of the transmitted wave η is related to the exit phase ξ_0^t as $\eta = \xi_0^t - dk_0$, where $d = z_R - z_L$. The Wigner time delay $\Delta\tau$ is the shift of the asymptotic $z \rightarrow \infty$ equation of motion relative to that of the free particle, see Fig. 1(d), and it equals the energy derivative of the phase η [26–28]: $\Delta\tau = \hbar d\eta/dE \equiv \dot{\eta}$.

If the slab has a symmetry operation \hat{s} that swaps the planes $z = z_L$ and $z = z_R$ then the following relation between reflection and transmission coefficients holds:

$$k_0 - \sum_{|\mathbf{g}| < k_0} k_{\mathbf{g}} |t_{\mathbf{g}} + r_{s\mathbf{g}}|^2 = 0, \quad (2)$$

where the sum runs over the propagating beams $|\mathbf{g}| < k_0$, i.e., real $k_{\mathbf{g}}$. The propagating secondary beams emerge at the energy $E_{\text{SB}} = \hbar^2 g_{\text{SB}}^2/2m$, where g_{SB} is the magnitude of the shortest nonzero \mathbf{g} -vector. Below E_{SB} , the current conservation law combined with Eq. (2) leads to the relation $\xi_0^t - \xi_0^r = \pm\pi/2$, which is well known for 1D

scattering [34]. For several propagating beams it acquires a more complicated form of a cosine sum rule

$$\sum_{|\mathbf{g}| < k_0} k_{\mathbf{g}} |t_{\mathbf{g}} r_{s\mathbf{g}}| \cos(\xi_{\mathbf{g}}^t - \xi_{s\mathbf{g}}^r) = 0. \quad (3)$$

An important identity relates the dwell time $\tilde{\tau}$ [28]

$$\tilde{\tau} = \frac{1}{v_0} \int_{z_L}^{z_R} |\Psi(\mathbf{r}_{\parallel}, z)|^2 dz, \quad (4)$$

to the Wigner time delay $\Delta\tau$ in the 1D case [28, 35]:

$$\tilde{\tau} = \Delta\tau + \frac{d}{v_0} + \frac{\text{Im } r_0}{k_0 v_0} = \Delta\tau + \tau_{\text{FM}} - \tau_{\text{SI}}. \quad (5)$$

Here $v_0 = \hbar k_0/m$ is the free-space velocity, so $\tau_{\text{FM}} = d/v_0$ is the free particle transit time and $\tau_{\text{SI}} = \hbar \text{Im } r_0/2E$ is a self-interference delay [4]. In the 3D case the definition (4) of the dwell time must be modified to include the probability density contained in the evanescent secondary beams in the whole space, see Eq. (B4)

$$\tilde{\tau}_{3\text{D}} \equiv \tilde{\tau} + \frac{1}{v_0} \sum_{|\mathbf{g}| > k_0} \frac{R_{\mathbf{g}} + T_{\mathbf{g}}}{2|k_{\mathbf{g}}|}, \quad (6)$$

where $T_{\mathbf{g}} = |t_{\mathbf{g}}|^2$ and $R_{\mathbf{g}} = |r_{\mathbf{g}}|^2$ are the partial transmissivities and reflectivities, respectively. The additional term is negligible well below E_{SB} , and at E_{SB} it diverges. Everywhere below E_{SB} , an analogue of Eq. (5) holds $\tilde{\tau}_{3\text{D}} = \Delta\tau + \tau_{\text{FM}} - \tau_{\text{SI}}$, and the general formula valid at all energies reads

$$\tilde{\tau}_{3\text{D}} = \frac{1}{v_0} \sum_{|\mathbf{g}| < k_0} \frac{\hbar k_{\mathbf{g}}}{m} (T_{\mathbf{g}} \dot{\xi}_{\mathbf{g}}^t + R_{\mathbf{g}} \dot{\xi}_{\mathbf{g}}^r) + \frac{\text{Im } r_0}{v_0 k_0}. \quad (7)$$

Equations (2) to (7) are derived in Appendix B.

Figure 2(a) shows transmission spectra for 1 to 6ML graphene and semi-infinite graphite. Clearly visible are conducting and reflecting intervals, evolving respectively into bulk bands and forbidden gaps of graphite. Each of the two lowest bands hosts $n - 1$ spikes ($T = 1$ resonances) for an n ML slab. They originate from interlayer scattering [37–39], hence are referred to as 1D bands. At the resonances, the transit time sharply peaks, see Fig. 3, similar to the resonant tunneling through a double barrier [40]. At low energies the larger velocity at the nuclei causes a faster propagation, as in the classical mechanics, so $\Delta\tau$ is on average negative, Fig. 2(c). In the upper 1D band, the band structure effect outweighs the classical acceleration leading to an overall positive slope of $\eta(E)$.

The N-band around 30 eV is related to a scattering resonance due to coupling of the in-plane and perpen-

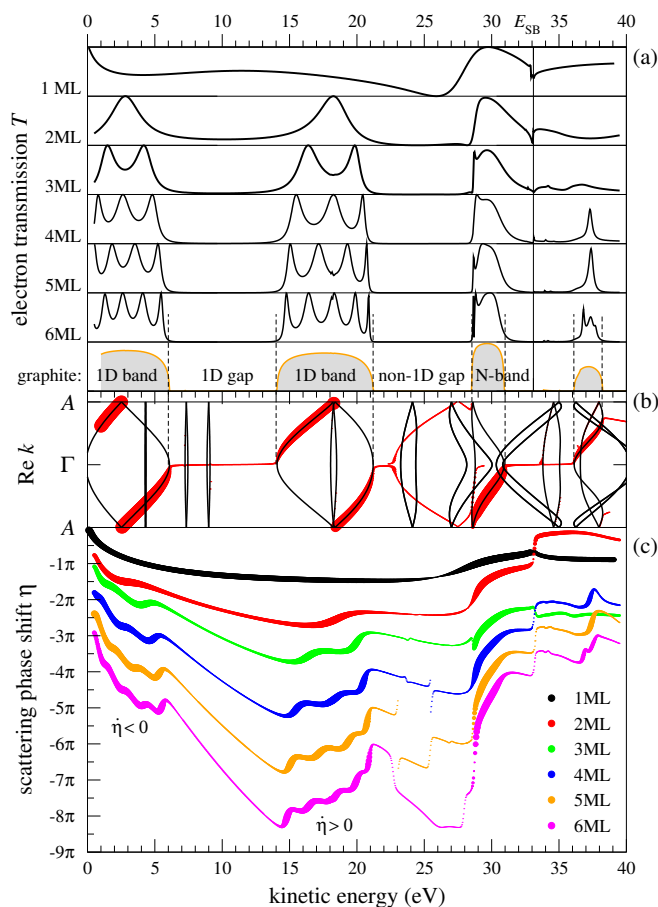


FIG. 2. (a) Transmission $T(E)$ through 1 to 6ML graphene and bulk graphite. T ranges from 0 to 1 in all the panels. (b) Black lines are the Γ A band structure of graphite. Red circles are the conducting complex band structure [36]: in the bulk, Ψ is a sum of propagating and evanescent Bloch waves, and size of the circle is proportional to the current carried by the partial wave. Black lines not marked by red circles are irrelevant for transmission. Red circles that do not mark any black lines are evanescent waves. (c) Scattering phase shift $\eta(E)$ for 1 to 6ML slabs. Size of the symbol is proportional to the transmission amplitude $|t_0|$ of the main beam, see Eq. (1).

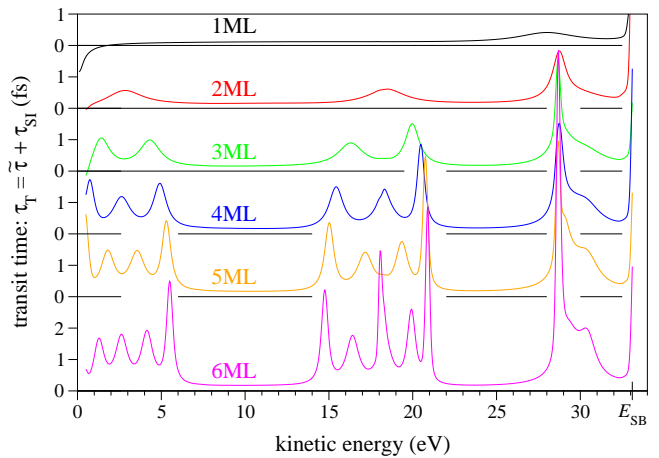


FIG. 3. Transit time through 1 to 6ML graphene slabs. Spectra are shown up to E_{SB} because Eq. (5) is used.

dicular motions [41, 42], and it behaves qualitatively differently from the 1D bands: there are no T -resonances, and the transit time is approximately proportional to the thickness d . In the band gaps transmission is effected by evanescent waves, so both the dwell time $\tilde{\tau}$ and self-interference time τ_{SI} [Eq. (5)] saturate with d , and so does the transit time $\tau_T = \Delta\tau + \tau_{FM}$: in the gap center $\tau_T^\infty = 180$ as in the lower and 190 as in the upper gap.

We have seen in Fig. 3 that the dwell time $\tilde{\tau}_{3D}$ diverges on approaching E_{SB} leading to a divergence of the Wigner time delay. Let us now focus on energies just above E_{SB} . There the simple relation $\xi_0^t - \xi_0^r = \pm\pi/2$ does not hold, and the general formula (7) should be used. We can write $\xi_0^t - \xi_0^r = \gamma(E) \pm \pi/2$, with $\gamma(E_{SB}) = 0$, and it follows from Eq. (3) that

$$k_0 |t_0 r_0| \sin(\gamma) = \sum_{0 < |\mathbf{g}| < k_0} k_{\mathbf{g}} |t_{\mathbf{g}} r_{\mathbf{sg}}| \cos(\xi_{\mathbf{g}}^t - \xi_{\mathbf{sg}}^r). \quad (8)$$

In the vicinity of E_{SB} , owing to the steeply growing $k_{\mathbf{g}}$, the energy derivative of γ diverges as $1/\sqrt{(E_{SB} - E)E}$. However, unlike the case of $E < E_{SB}$, the sign of the divergent term may be different in different systems. This divergence turns out to lead to negative time delay in particular in graphene, h-BN, and a monolayer oxygen in the geometry of ruthenium surface oxide [43], see Fig. 4.

Above the respective E_{SB} energies the three monolayers have similar shape of both $T(E)$ and $\Delta\tau(E)$ curves, with $\Delta\tau(E)$ diverging toward $-\infty$. This nontrivial speed-up cannot be predicted from the general theory, so we have validated its consistency by comparing $\Delta\tau$ obtained as $\dot{\eta}_0$ with the value derived from the phase derivatives of the propagating secondary beams $\dot{\xi}_{\mathbf{g}}^r$ and $\dot{\xi}_{\mathbf{g}}^t$ and the density integral $\tilde{\tau}_{3D}$ through Eq. (7). For all three systems the discrepancies in $\Delta\tau$ are negligible over the entire range considered, see Fig. 6

In the language of the Hartman effect, i.e., if one assumes that the wave packet can be ascribed a trajectory,

unlimited negative time delay implies negative transit time, which illustrates that τ_T has no physical meaning. Nevertheless, for a sufficiently spectrally narrow wave packet this effect can be measured as a substantial reduction of the arrival time, the essential novel aspect being that no stop band is involved, and consequently the transmitted fraction of the current is orders of magnitude larger than in tunneling—above 50%, see Figs. 4(a) and 4(c). A spectrally wide packet with energy around E_{SB} will be torn into two spatially separated ones with comparable intensities.

The $\Delta\tau$ -divergence due to the emergence of the secondary beams is a general phenomenon, with E_{SB} depending solely on the surface Bravais lattice, so it is to be expected for any exfoliated material. Apart from that, the atomic structure of a specific multilayer may bring about additional strong features: One example is the broad $\Delta\tau$ maximum at 28 eV due to the N-resonance in graphene and h-BN. Furthermore, the more complicated geometry of h-BN gives rise to a deep $T(E)$ minimum at 8 eV and a sharp resonance at 20 eV [manifested by a steep drop of $T(E)$], see Fig. 4(a), both structures manifesting a significant increase of $\Delta\tau$, see Fig. 4(b). The absence of the N-resonance in oxygen monolayer, Fig. 4(c), is ex-

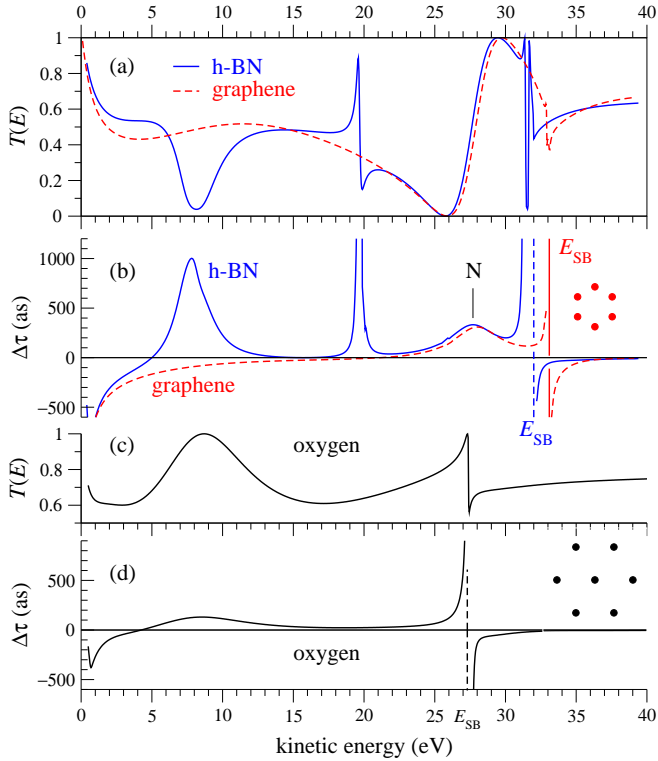


FIG. 4. (a) Transmissivity $T(E)$ of 1ML graphene [red dashed line, same as the upper curve in Fig. 2(a)] compared to 1ML h-BN (blue). (b) Wigner delay $\Delta\tau$ for graphene (red) and h-BN (blue). (c) $T(E)$ for 1ML oxygen (hexagonal structure [43]). (d) $\Delta\tau$ for 1ML oxygen. Vertical bars indicate critical energies E_{SB} . Circles in the insets show fragments of the lattices of graphene (red) and oxygen (black).

plained by its simple hexagonal geometry in contrast to the honeycomb lattice of graphene and h-BN. However, the oxygen monolayer manifests the same type of divergence at E_{SB} as the other materials. One may expect the more complicated 2D structures, such as transition metal dichalcogenids, to show more interesting features.

The general formula (8) proves the divergence of the derivative of the phase difference between transmission and reflection. We will now present a simple 2D model, for which the divergence of the phase derivatives $\dot{\xi}_0^t$ and $\dot{\xi}_0^r$ themselves can be demonstrated analytically. Consider an infinite chain of atoms along \hat{x} axis modeled by a δ -function potential $\Omega\delta(y)$ in the \hat{y} direction and a weak corrugation $\cos(g_{\text{SB}}x)$ along \hat{x} : $\hat{H} = (\hat{p}_x^2 + \hat{p}_y^2)/2m + 2(\hbar^2/m)\Omega\delta(y)\cos(g_{\text{SB}}x)$. The $\cos(g_{\text{SB}}x)$ perturbation couples the motions along \hat{x} and \hat{y} and gives rise to the secondary beams at $E_{\text{SB}} = \hbar^2 g_{\text{SB}}^2/2m$.

By applying the Lippmann-Schwinger equation to the Laue representation of the wave function for normal incidence (along \hat{y}), $\Psi(x, y) = \sum_g \phi_g(y) \exp(igx)$, we obtain the central beam wave function in terms of the Green's function for a 1D free motion $G_0^{\text{1D}}(y; \omega)$ [44]:

$$\phi_0(y) = \exp(iky) - \frac{2i\Omega \exp(ik|y|)}{k(F_{g_{\text{SB}}}^{-1} - 2F_0 - F_{2g_{\text{SB}}})}, \quad (9)$$

where $F_g \equiv \hbar^2 \Omega G_0^{\text{1D}}(0; k^2 - g^2)/m$, see Appendix C. Equation (C9) yields the reflection and transmission amplitudes: $r = -2i\Omega/[k(F_{g_{\text{SB}}}^{-1} - 2F_0 - F_{2g_{\text{SB}}})]$ and $t = 1 + r$. Around E_{SB} , it can be proved that $F_{g_{\text{SB}}}^{-1} = -\sqrt{g_{\text{SB}}^2 - k^2}/\Omega$ for $g_{\text{SB}}^2 > k^2$ and $F_{g_{\text{SB}}}^{-1} = i\sqrt{k^2 - g_{\text{SB}}^2}/\Omega$ for $g_{\text{SB}}^2 < k^2$, see Appendix C. The other two parameters F_g in Eq. (C9) become $F_0 = -i\Omega/g_{\text{SB}}$ and $F_{2g_{\text{SB}}} = -\Omega/(g_{\text{SB}}\sqrt{3})$, so $\Delta\tau$ becomes

$$\Delta\tau \approx \frac{m}{\hbar\beta} \times \begin{cases} \frac{6g_{\text{SB}}^2\Omega^2}{13(\Omega^2 - \beta\sqrt{3})^2}, & E < E_{\text{SB}}, \\ \frac{12\sqrt{3}g_{\text{SB}}^2\Omega^4(\Omega^2 + \beta)}{13[\Omega^4 + 3\beta(\Omega^2 + \beta)]^2}, & E > E_{\text{SB}}, \end{cases} \quad (10)$$

where $\beta \equiv (2m/\hbar^2)\sqrt{E_{\text{SB}}|E - E_{\text{SB}}|}$ yields the divergence of the Wigner time delay, cf. Eq. (8).

To summarize, our study has revealed hitherto unknown phenomena caused by the in-plane umklapp scattering, which are especially conspicuous in monolayers: the steep increase of the delay at the transmission minima in h-BN and, most strikingly, the divergent delay followed by divergent advance of the central beam due to the emergence of the secondary beams observed in the monolayers of graphene, h-BN, and oxygen. In thicker multilayers, the lateral scattering damps the sharp T -resonances and eliminates the related huge time delays.

The rapid energy variations of the time delay cause a spatial reshaping of the wave packet, which can be employed to experimentally study the details of the acceleration of the outgoing photoelectrons by a spatially inhomogeneous infrared laser field at the surface. This is an

insufficiently studied question, both experimentally and theoretically, and the usual assumption is to neglect the spatial extent of the outgoing wave packet [17–24]. The possibility to split the wave packet into two—separated by a fraction of a femtosecond—and observe their acceleration by the same probe pulse opens a way to clarify the details of the streaking mechanism, which is instrumental for the interpretation of the measurements. Such a possibility is offered by a thin overlayer in which the time delay rapidly changes with energy due to a specific crystal structure (as in h-BN) or due to the emergence of the secondary beams, common to all crystalline films. The advantage over the traditional Hartman effect is that the in-plane scattering induced $\Delta\tau$ resonances are not accompanied by a dramatic drop of the transmitted flux. In addition, owing to the minimal thickness of a monoatomic overlayer, the streaking field is minimally disturbed. One may argue that the phase time that underlies the present study is an asymptotic value, and the extrapolation of the $z \rightarrow \infty$ equation of motion to the vicinity of the scatterer is not rigorously justified [2, 32] (even though this is quite common, see, e.g., Refs. [14, 15, 45] and an analysis in Ref. [46]). Still, our numerical streaking experiment [47] showed that the photoelectron escape time extracted from streaking reflected all the band-structure related features of the relevant phase time, and even the absolute values were reasonably close. Thus, our present results offer a promising starting point to study the wave-packet speed-up unrelated to tunneling.

Apart from the practical applications, the discovered properties of the ultrathin layers may be interesting from the point of view of developing quantum-mechanical formalisms in which the motion of the quantum particle is considered in terms of trajectories [48–50].

ACKNOWLEDGMENTS

This work was supported by the Spanish Ministry of Science and Innovation (MICINN Project No. PID2022-139230NB-I00) and by the National Academy of Sciences of Ukraine (Project No. III-2-22 and III-4-23).

Appendix A: Calculation of scattering states

The crystal potential is constructed within the local density approximation; it includes both the Coulomb singularities at the nuclei and a realistic full-potential shape everywhere between z_L and z_R . In the scattering region an all-electron wave function Ψ is a linear combination of the Bloch eigenfunctions of an auxiliary band structure problem for a periodic supercell extending from $-c/2$ to $c/2$, see Fig. 5. Then the wave function is Fourier expanded to arrive at the Laue representation

$$\Psi(\mathbf{r}_{\parallel}, z) = \sum_{\mathbf{g}} \phi_{\mathbf{g}}(z) \exp[i\mathbf{g}\mathbf{r}_{\parallel}], \quad (\text{A1})$$

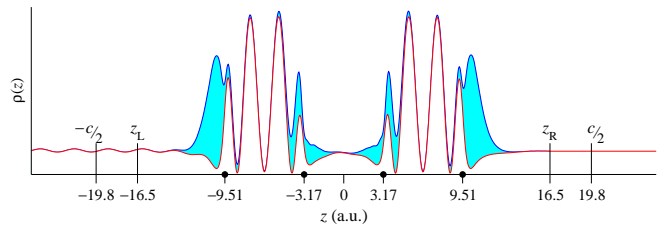


FIG. 5. Probability density profile $\rho(z)$ of the scattering wave function for normal incidence on a 4ML graphene film at 18.24 eV kinetic energy, corresponding to a transmission resonance, see Fig. 6. Blue line is the total density and red line is the $\mathbf{g} = 0$ contribution $|\phi_0(z)|^2$, see Eq. (A1). The cyan shaded area shows the contribution from the $\mathbf{g} \neq 0$ Fourier harmonics. The artificial supercell extends from $-c/2$ to $c/2$. Black circles show the location of the four graphene planes.

so the density profile $\rho(z)$ of the scattering state is $\rho(z) = \sum_{\mathbf{g}} |\phi_{\mathbf{g}}(z)|^2$. An example for the normal incidence on a 4ML graphene slab at $E = 18.24$ eV is shown in Fig. 5. Some more details of the application of the method to graphene monolayer and bilayer have been presented in refs. [41, 51, 52].

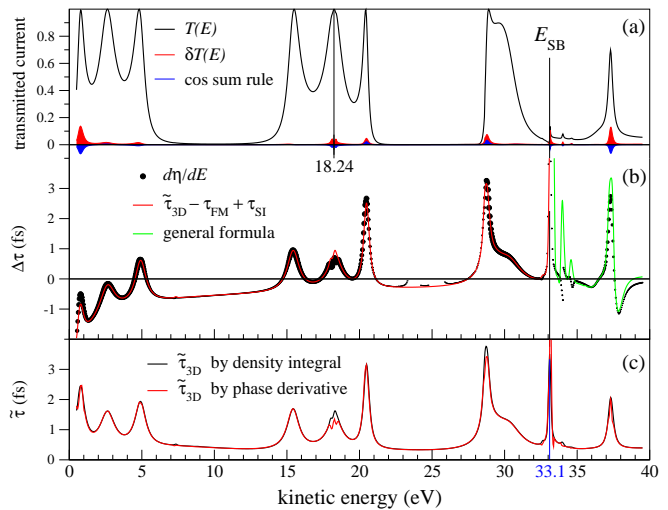


FIG. 6. (a) Total current $T(E)$ through 4ML graphene (black curve), current nonconservation δT (red shading), and sum rule (3) (blue shading). (b) Delay $\Delta\tau$ as the energy derivative $\dot{\eta}$ (black circles), from the analogue of Eq. (5), $\tilde{\tau}_{3D} = \Delta\tau + \tau_{FM} - \tau_{SI}$, below E_{SB} (red), and from the general formula (7) above E_{SB} (green). Size of the circle is proportional to $|t_0|$. Below E_{SB} agreement between the two curves depends on the phase relation $\xi_0^t - \xi_0^r = \pm\pi/2$. (c) Dwell time (6) (black) compared to the right hand side of Eq. (7) (red).

The variational method for scattering [29] is based on minimizing the functional $\|(\hat{H} - E)\Psi\|$, so the solution (A1) satisfies the Schrödinger equation only with certain accuracy. Identities (2)–(7) allow us to estimate the computational uncertainty and verify that it is much smaller than the physically relevant quantities.

Figure 6(a) shows the total current spectrum

$$T(E) = \sum_{|\mathbf{g}| < k_0} T_{\mathbf{g}}(E) k_{\mathbf{g}} / k_0 \quad (\text{A2})$$

together with the current nonconservation $\delta T(E)$ defined as the difference of the probability fluxes at z_L and z_R . The parameter δT is a good indicator of the overall quality of the wave function: for 4MLs its average value over the range of 40 eV is below 1%, and it sharply peaks to exceed 5% in a few narrow intervals, accompanied by a slight violation of the identities (3), (6), or (7).

Computationally, dwell time $\tilde{\tau}$ is the most reliable quantity, so below E_{SB} the delay $\Delta\tau$ can be obtained without resorting to numerical differentiation. This is especially important when T_0 drops below 10^{-6} , whereby its phase ξ_0^t becomes highly unreliable, as, e.g., between 22 and 27 eV in Fig. 6(b). The uncertainties are of similar magnitude for the 3, 5, and 6MLs, and they are much smaller (practically negligible) for 1 and 2MLs. Thus, the accuracy of $\Delta\tau$ is sufficiently high to enable a detailed analysis of scattering by multilayers.

Appendix B: Phases and dwell time in 3D case

According to Eq. (1) of the main text, the wave function for a wave incident from the left in the left half-space reads

$$\Psi_{\rightarrow}(\mathbf{r}_{\parallel}, z) = \exp ik_0 z + \sum_{\mathbf{g}} r_{\mathbf{g}} \exp i[-k_{\mathbf{g}}(z - z_L) + \mathbf{g}\mathbf{r}_{\parallel}].$$

Also, it follows from Eq. (1) that for a symmetric crystal the wave incident from the right in the left half-space is

$$\Psi_{\leftarrow}(\mathbf{r}_{\parallel}, z) = \sum_{\mathbf{g}} t_{\mathbf{g}} \exp i[-k_{\mathbf{g}}(z - z_L) + \mathbf{g}\mathbf{r}_{\parallel}].$$

$$\text{left boundary: } \phi_{\mathbf{g}}^*(z_L) = \delta_{0\mathbf{g}} + r_{\mathbf{g}}^*,$$

$$\dot{\phi}_{\mathbf{g}}(z_L) = \dot{r}_{\mathbf{g}},$$

$$\dot{\phi}'_{\mathbf{g}}(z_L) = i(\delta_{0\mathbf{g}} \dot{k}_0 - k_{\mathbf{g}} \dot{r}_{\mathbf{g}} - r_{\mathbf{g}} \dot{k}_{\mathbf{g}}),$$

$$\phi_{\mathbf{g}}'^*(z_L) = i(-\delta_{0\mathbf{g}} k_0 + r_{\mathbf{g}}^* k_{\mathbf{g}}^*),$$

$$\text{right boundary: } \phi_{\mathbf{g}}^*(z_R) = t_{\mathbf{g}}^*,$$

$$\dot{\phi}_{\mathbf{g}}(z_R) = \dot{t}_{\mathbf{g}},$$

$$\dot{\phi}'_{\mathbf{g}}(z_R) = i(k_{\mathbf{g}} \dot{t}_{\mathbf{g}} + t_{\mathbf{g}} \dot{k}_{\mathbf{g}}),$$

$$\phi_{\mathbf{g}}'^*(z_R) = -it_{\mathbf{g}}^* k_{\mathbf{g}}^*,$$

(B5)

where $k_{\mathbf{g}}^* = k_{\mathbf{g}}$ for propagating beams and $k_{\mathbf{g}}^* = -k_{\mathbf{g}}$ for evanescent beams. Then Eq. (B4) becomes

$$\frac{2m}{\hbar^2} Q = ik_0 + 2k_0 \text{Im} r_0 - i \sum_{|\mathbf{g}| < k_0} 2(\dot{r}_{\mathbf{g}} r_{\mathbf{g}}^* + \dot{t}_{\mathbf{g}} t_{\mathbf{g}}^*) k_{\mathbf{g}} + (R_{\mathbf{g}} + T_{\mathbf{g}}) \dot{k}_{\mathbf{g}} - i \sum_{|\mathbf{g}| > k_0} (R_{\mathbf{g}} + T_{\mathbf{g}}) \dot{k}_{\mathbf{g}}, \quad (\text{B6})$$

where $R_{\mathbf{g}} = r_{\mathbf{g}} r_{\mathbf{g}}^*$ and $T_{\mathbf{g}} = t_{\mathbf{g}} t_{\mathbf{g}}^*$ are partial reflection and transmission probabilities. From the current conservation law $\frac{d}{dE} \sum_{|\mathbf{g}| < k_0} (r_{\mathbf{g}} r_{\mathbf{g}}^* + t_{\mathbf{g}} t_{\mathbf{g}}^*) k_{\mathbf{g}} = \dot{k}_0$ it follows that $\sum_{|\mathbf{g}| < k_0} (\dot{r}_{\mathbf{g}} r_{\mathbf{g}}^* + \dot{t}_{\mathbf{g}} t_{\mathbf{g}}^*) k_{\mathbf{g}} + (R_{\mathbf{g}} + T_{\mathbf{g}}) \dot{k}_{\mathbf{g}} = \dot{k}_0 - \sum_{|\mathbf{g}| < k_0} (r_{\mathbf{g}} \dot{r}_{\mathbf{g}}^* + t_{\mathbf{g}} \dot{t}_{\mathbf{g}}^*) k_{\mathbf{g}}$,

The superposition $\Psi_L = \Psi_{\rightarrow} + \Psi_{\leftarrow}$ carries zero current, and in vacuum the condition $\text{Re} \int \Psi_L^* (-i\partial\Psi_L/\partial z) d\mathbf{r}_{\parallel} = 0$ results in the relation

$$k_0[r_0 t_0^* + t_0 r_0^*] + \sum_{0 < |\mathbf{g}| < k_0} k_{\mathbf{g}} |t_{\mathbf{g}} + r_{\mathbf{g}}|^2 = 0, \quad (\text{B1})$$

where the sum is over the propagating secondary beams. This leads to Eq. (5). Below E_{SB} equation (B1) reduces to $\text{Re}(t_0 r_0^*) = 0$, which implies $\cos(\xi_0^t - \xi_0^r) = 0$ or $\xi_0^t - \xi_0^r = \pm\pi/2$, as in the 1D case [34]. For several propagating beams Eq. (B1) leads to Eq. (6).

Next we derive the expression for the dwell time in the 3D case. We follow the original derivation by Smith [28]: From the Schrödinger equation $\hat{H}\Psi = E\Psi$ and its energy derivative $(\hat{H} - E)\dot{\Psi} = \Psi$ we obtain

$$-\frac{\hbar^2}{2m} (\Psi^* \Delta \dot{\Psi} - \dot{\Psi} \Delta \Psi^*) = \Psi^* \Psi. \quad (\text{B2})$$

After integrating over \mathbf{r}_{\parallel} , the \mathbf{r}_{\parallel} part of the Laplacian in the left-hand side vanishes, $\sum_{\mathbf{g}} (\phi_{\mathbf{g}}^* \dot{\phi}_{\mathbf{g}} - \dot{\phi}_{\mathbf{g}} \phi_{\mathbf{g}}^*) |\mathbf{g}|^2 = 0$, and in the Laue representation (A1) equation (B2) becomes

$$-\frac{\hbar^2}{2m} \sum_{\mathbf{g}} \frac{d}{dz} (\phi_{\mathbf{g}}^* \dot{\phi}'_{\mathbf{g}} - \dot{\phi}_{\mathbf{g}} \phi_{\mathbf{g}}'^*) = \rho(z), \quad (\text{B3})$$

where the prime stands for the derivative d/dz and $\rho(z)$ is the density distribution profile. Integrating Eq. (B3) from z_L to z_R we obtain

$$-\frac{\hbar^2}{2m} \sum_{\mathbf{g}} (\phi_{\mathbf{g}}^* \dot{\phi}'_{\mathbf{g}} - \dot{\phi}_{\mathbf{g}} \phi_{\mathbf{g}}'^*) \Big|_{z_L}^{z_R} = \int_{z_L}^{z_R} \rho(z) dz \equiv Q. \quad (\text{B4})$$

Let us express the boundary values in terms of the notation of Eqs. (1) and (2)

which we substitute into the $|\mathbf{g}| < k_0$ sum of (B6) to obtain

$$\frac{2m}{\hbar^2}Q = 2k_0 \text{Im } r_0 - i \sum_{|\mathbf{g}| < k_0} (\dot{r}_{\mathbf{g}} r_{\mathbf{g}}^* + \dot{t}_{\mathbf{g}} t_{\mathbf{g}}^* - \dot{r}_{\mathbf{g}}^* r_{\mathbf{g}} - \dot{t}_{\mathbf{g}}^* t_{\mathbf{g}}) k_{\mathbf{g}} - i \sum_{|\mathbf{g}| > k_0} (R_{\mathbf{g}} + T_{\mathbf{g}}) \dot{k}_{\mathbf{g}}. \quad (\text{B7})$$

Using the identity $\text{Im}(\dot{r}_{\mathbf{g}} r_{\mathbf{g}}^* + \dot{t}_{\mathbf{g}} t_{\mathbf{g}}^*) = R_{\mathbf{g}} \dot{\xi}_{\mathbf{g}}^r + T_{\mathbf{g}} \dot{\xi}_{\mathbf{g}}^t$ and the derivatives of the wave vectors $\dot{k}_{\mathbf{g}} = \frac{m}{\hbar^2 k_{\mathbf{g}}}$, we obtain

$$\tilde{\tau} = \frac{\text{Im } r_0}{k_0 v_0} + \frac{\hbar}{v_0} \sum_{|\mathbf{g}| < k_0} (R_{\mathbf{g}} \dot{\xi}_{\mathbf{g}}^r + T_{\mathbf{g}} \dot{\xi}_{\mathbf{g}}^t) v_{\mathbf{g}} - \frac{1}{v_0} \sum_{|\mathbf{g}| > k_0} \frac{R_{\mathbf{g}} + T_{\mathbf{g}}}{2|k_{\mathbf{g}}|}, \quad (\text{B8})$$

where for the evanescent waves $|k_{\mathbf{g}}| = \sqrt{\hbar^2 |\mathbf{g}|^2 / 2m - E}$. The $|\mathbf{g}| > k_0$ sum in Eq. (B8) is the integral probability density stored in the evanescent tails of Ψ in both half-spaces outside the region technically assigned to the

scatterer. Thus, it is natural to unite the last term in Eq. (B8) with $\tilde{\tau}$ and introduce $\tilde{\tau}_{3\text{D}}$, see Eq. (6), which yields Eq. (7)

Appendix C: 2D Nearly-free-electron model analysis

We consider the Hamiltonian

$$\hat{H} = \frac{\hat{p}_x^2 + \hat{p}_y^2}{2m} + 2 \frac{\hbar^2}{m} \Omega \delta(y) \cos(g_{\text{SB}} x). \quad (\text{C1})$$

The Lippmann–Schwinger equation for the wave function for a normal incidence (along $\hat{\mathbf{y}}$) on the chain reads

$$\Psi(x, y) = \exp(iky) + \frac{\hbar^2}{m} \int dx' G_0^{2\text{D}}(x - x', y; k^2) 2\Omega \cos(g_{\text{SB}} x') \Psi(x', 0), \quad (\text{C2})$$

$$\text{where } G_0^{2\text{D}}(x, y; \omega) = \frac{2m}{\hbar^2} \iint \frac{dq_x dq_y}{4\pi^2} \frac{\exp(iq_x x + iq_y y)}{\omega - q_x^2 - q_y^2}$$

is the Green's function for a 2D free motion. Substituting the Laue representation (A1) in both sides of Eq. (C2) yields

$$\Psi(x, y) = \exp(iky) + \frac{\hbar^2}{m} \Omega \sum_g \phi_g \left\{ \exp[i(g + g_{\text{SB}})x] G_0^{1\text{D}}[y; k^2 - (g + g_{\text{SB}})^2] + \exp[i(g - g_{\text{SB}})x] G_0^{1\text{D}}[y; k^2 - (g - g_{\text{SB}})^2] \right\}, \quad (\text{C3})$$

where $\phi_g \equiv \phi_g(y=0)$ and $G_0^{1\text{D}}(y; \omega)$ is the Green's function for a free motion in one dimension [44],

$$G_0^{1\text{D}}(y, \omega) = \begin{cases} -\frac{m}{\hbar^2 q} \exp(-q|y|), & \omega < 0, \\ -\frac{im}{\hbar^2 q} \exp(iq|y|), & \omega > 0, \end{cases} \quad (\text{C4})$$

where $q \equiv \sqrt{|\omega|}$. It follows from Eq. (C4) that for $y \rightarrow \pm\infty$, in the Laue representation (C3) of $\Psi(x, y)$ one can retain only propagating terms, i.e., those with the positive ω argument of $G_0^{1\text{D}}$. Then, around E_{SB} , we have

$$\Psi(x, y) = e^{iky} + \frac{\hbar^2}{m} \Omega \left\{ (\phi_{g_{\text{SB}}} + \phi_{-g_{\text{SB}}}) G_0^{1\text{D}}(y; k^2) + [2\phi_0 \cos(g_{\text{SB}} x) + \phi_{2g_{\text{SB}}} e^{ig_{\text{SB}} x} + \phi_{-2g_{\text{SB}}} e^{-ig_{\text{SB}} x}] G_0^{1\text{D}}(y; \epsilon) \right\},$$

where $\epsilon \equiv k^2 - g_{\text{SB}}^2$. The central beam scattering is given

by the first term in the rectangular brackets.

$$\phi_0(y) = \exp(iky) - \frac{i\Omega \exp(ik|y|)}{k} (\phi_{g_{\text{SB}}} + \phi_{-g_{\text{SB}}}). \quad (\text{C5})$$

Equating the coefficients of the Fourier harmonics $\exp(igx)$ in Eq. (C3) we obtain

$$\phi_g = \delta_{g0} + (\phi_{g-g_{\text{SB}}} + \phi_{g+g_{\text{SB}}}) F_g, \quad (\text{C6})$$

$$F_g \equiv \frac{\hbar^2}{m} \Omega G_0^{\text{1D}}(0; k^2 - g^2). \quad (\text{C7})$$

If the potential is small compared with the kinetic energy E_{SB} and oscillates sufficiently rapidly, $\Omega/g_{\text{SB}} \ll 1$, a nearly-free-electron approximation may be applied, i.e., only the shortest- g terms retained in the Laue representation: $g = 0, \pm g_{\text{SB}}, \pm 2g_{\text{SB}}$. By truncating the chain of equations (C6) at $\phi_{\pm 2g_{\text{SB}}}$ we find

$$\phi_{g_{\text{SB}}} = \phi_{-g_{\text{SB}}} \approx \frac{1}{F_{g_{\text{SB}}}^{-1} - (2F_0 + F_{2g_{\text{SB}}})}. \quad (\text{C8})$$

Finally, we substitute $\phi_{\pm g_{\text{SB}}}$ into Eq. (C5) to obtain

$$\phi_0(y) = \exp(iky) - \frac{2i\Omega \exp(ik|y|)}{k(F_{g_{\text{SB}}}^{-1} - 2F_0 - F_{2g_{\text{SB}}})}, \quad (\text{C9})$$

which is Eq. (9) of the main text. Equation (C9) yields the reflection and transmission amplitudes: $r = -2i\Omega/[k(F_{g_{\text{SB}}}^{-1} - 2F_0 - F_{2g_{\text{SB}}})]$ and $t = 1 + r$. In the vicinity of E_{SB} it holds $\epsilon/g_{\text{SB}}^2 \ll 1$, and we may set $\epsilon = 0$ in all terms except

$$F_{g_{\text{SB}}}^{-1} = \begin{cases} -\sqrt{|\epsilon|}/\Omega, & \epsilon < 0, \\ i\sqrt{\epsilon}/\Omega, & \epsilon > 0. \end{cases} \quad (\text{C10})$$

Then, in the limit $k \rightarrow g_{\text{SB}}$ the coefficients F_g in Eq. (C9) become $F_0 \rightarrow -i\Omega/g_{\text{SB}}$ and $F_{2g_{\text{SB}}} \rightarrow -\Omega/(g_{\text{SB}}\sqrt{3})$, and we obtain expressions (10) for $\Delta\tau$, which demonstrate the divergence of the Wigner time delay for $\epsilon \rightarrow 0$, i.e. for $E \rightarrow E_{\text{SB}}$.

-
- [1] T. E. Hartman, Tunneling of a wave packet, *J. Appl. Phys.* **33**, 3427 (1962).
- [2] E. H. Hauge and J. A. Støvneng, Tunneling times: a critical review, *Rev. Mod. Phys.* **61**, 917 (1989).
- [3] R. Landauer and T. Martin, Barrier interaction time in tunneling, *Rev. Mod. Phys.* **66**, 217 (1994).
- [4] H. G. Winful, Tunneling time, the Hartman effect, and superluminality: A proposed resolution of an old paradox, *Physics Reports* **436**, 1 (2006).
- [5] R. S. Dumont, T. Rivlin, and E. Pollak, The relativistic tunneling flight time may be superluminal, but it does not imply superluminal signaling, *New Journal of Physics* **22**, 093060 (2020).
- [6] G. E. Field, On the status of quantum tunnelling time, *European Journal for Philosophy of Science* **12**, 57 (2022).
- [7] A. M. Steinberg, P. G. Kwiat, and R. Y. Chiao, Measurement of the single-photon tunneling time, *Phys. Rev. Lett.* **71**, 708 (1993).
- [8] A. Enders and G. Nimtz, Evanescent-mode propagation and quantum tunneling, *Phys. Rev. E* **48**, 632 (1993).
- [9] C. Spielmann, R. Szipöcs, A. Stingl, and F. Krausz, Tunneling of optical pulses through photonic band gaps, *Phys. Rev. Lett.* **73**, 2308 (1994).
- [10] P. Balcou and L. Dutriaux, Dual optical tunneling times in frustrated total internal reflection, *Phys. Rev. Lett.* **78**, 851 (1997).
- [11] J. J. Carey, J. Zawadzka, D. A. Jaroszynski, and K. Wynne, Noncausal time response in frustrated total internal reflection?, *Phys. Rev. Lett.* **84**, 1431 (2000).
- [12] S. Longhi, M. Marano, P. Laporta, and M. Belmonte, Superluminal optical pulse propagation at $1.5\mu\text{m}$ in periodic fiber Bragg gratings, *Phys. Rev. E* **64**, 055602 (2001).
- [13] A. S. Landsman, M. Weger, J. Maurer, R. Boge, A. Ludwig, S. Heuser, C. Cirelli, L. Gallmann, and U. Keller, Ultrafast resolution of tunneling delay time, *Optica* **1**, 343 (2014).
- [14] P. Eckle, A. N. Pfeiffer, C. Cirelli, A. Staudte, R. Dörner, H. G. Muller, M. Büttiker, and U. Keller, Attosecond ionization and tunneling delay time measurements in helium, *Science* **322**, 1525 (2008).
- [15] U. S. Sainadh, H. Xu, X. Wang, A. Atia-Tul-Noor, W. C. Wallace, N. Douguet, A. Bray, I. Ivanov, K. Bartschat, A. Kheifets, R. T. Sang, and I. V. Litvinyuk, Attosecond angular streaking and tunnelling time in atomic hydrogen, *Nature* **568**, 75 (2019).
- [16] R. Ramos, D. Spierings, I. Racicot, and A. M. Steinberg, Measurement of the time spent by a tunnelling atom within the barrier region, *Nature* **583**, 529 (2020).
- [17] A. L. Cavalieri, N. Mueller, T. Uphues, V. S. Yakovlev, A. Baltuska, B. Horvath, B. Schmidt, L. Bluemel, R. Holzwarth, S. Hendel, M. Drescher, U. Kleineberg, P. M. Echenique, R. Kienberger, F. Krausz, and U. Heinzmann, Attosecond spectroscopy in condensed matter, *Nature* **449**, 1029 (2007).
- [18] M. Schultze, M. Fieß, N. Karpowicz, J. Gagnon, M. Korbman, M. Hofstetter, S. Neppl, A. L. Cavalieri, Y. Komninos, T. Mercouris, C. A. Nicolaides, R. Pazourek, S. Nagele, J. Feist, J. Burgdörfer, A. M. Azzeer, R. Ernstorfer, R. Kienberger, U. Kleineberg, E. Goulielmakis, F. Krausz, and V. S. Yakovlev, Delay in photoemission, *Science* **328**, 1658 (2010).
- [19] S. Neppl, R. Ernstorfer, E. M. Bothschafter, A. L. Cavalieri, D. Menzel, J. V. Barth, F. Krausz, R. Kienberger, and P. Feulner, Attosecond time-resolved photoemission from core and valence states of magnesium, *Phys. Rev. Lett.* **109**, 087401 (2012).
- [20] S. Neppl, R. Ernstorfer, A. L. Cavalieri, C. Lemell, G. Wachter, E. Magerl, E. M. Bothschafter, M. Jobst, M. Hofstetter, U. Kleineberg, J. V. Barth, D. Menzel, J. Burgdörfer, P. Feulner, F. Krausz, and R. Kienberger, Direct observation of electron propagation and dielectric screening on the atomic length scale, *Nature* **517**, 342 (2015).
- [21] W. A. Okell, T. Witting, D. Fabris, C. A. Arrell, J. Hengster, S. Ibrahimkutty, A. Seiler, M. Barthelmeß,

- S. Stankov, D. Y. Lei, Y. Sonnefraud, M. Rahmani, T. Uphues, S. A. Maier, J. P. Marangos, and J. W. G. Tisch, Temporal broadening of attosecond photoelectron wavepackets from solid surfaces, *Optica* **2**, 383 (2015).
- [22] F. Siek, S. Neb, P. Bartz, M. Hensen, C. Strüber, S. Fiechter, M. Torrent-Sucarrat, V. M. Silkin, E. E. Krasovskii, N. M. Kabachnik, S. Fritzsche, R. D. Muiño, P. M. Echenique, A. K. Kazansky, N. Müller, W. Pfeiffer, and U. Heinzmann, Angular momentum-induced delays in solid-state photoemission enhanced by intra-atomic interactions, *Science* **357**, 1274 (2017), <https://www.science.org/doi/pdf/10.1126/science.aam9598>.
- [23] M. Ossiander, J. Riemensberger, S. Neppl, M. Mittermair, M. Schäffer, A. Duensing, M. S. Wagner, R. Heider, M. Wurzer, M. Gerl, M. Schnitzenbaumer, J. V. Barth, F. Libisch, C. Lemell, J. Burgdörfer, P. Feulner, and R. Kienberger, Absolute timing of the photoelectric effect, *Nature* **561**, 374 (2018).
- [24] J. Riemensberger, S. Neppl, D. Potamianos, M. Schäffer, M. Schnitzenbaumer, M. Ossiander, C. Schröder, A. Guggenmos, U. Kleineberg, D. Menzel, F. Allegretti, J. V. Barth, R. Kienberger, P. Feulner, A. G. Borisov, P. M. Echenique, and A. K. Kazansky, Attosecond dynamics of *sp*-band photoexcitation, *Phys. Rev. Lett.* **123**, 176801 (2019).
- [25] R. Pazourek, S. Nagele, and J. Burgdörfer, Attosecond chronoscopy of photoemission, *Rev. Mod. Phys.* **87**, 765 (2015).
- [26] D. Bohm, *Quantum Theory* (Prentice-Hall, New York, 1951).
- [27] E. P. Wigner, Lower limit for the energy derivative of the scattering phase shift, *Phys. Rev.* **98**, 145 (1955).
- [28] F. T. Smith, Lifetime matrix in collision theory, *Phys. Rev.* **118**, 349 (1960).
- [29] E. E. Krasovskii, Augmented-plane-wave approach to scattering of Bloch electrons by an interface, *Phys. Rev. B* **70**, 245322 (2004).
- [30] J. Muga, S. Brouard, and D. Macias, Time of arrival in quantum mechanics, *Annals of Physics* **240**, 351 (1995).
- [31] C. Anastopoulos and N. Savvidou, Quantum temporal probabilities in tunneling systems, *Annals of Physics* **336**, 281 (2013).
- [32] E. H. Hauge, *Can one speak about tunneling times in polite society?* (World Scientific, 1997) pp. 1–17, Proceedings of the Adriatico research conference on tunneling and its implications; Trieste (Italy); 30 Jul - 2 Aug 1996.
- [33] D. Sokolovski and E. Akhmatskaya, No time at the end of the tunnel, *Communications Physics* **1**, 47 (2018).
- [34] J. P. Falck and E. H. Hauge, Larmor clock reexamined, *Phys. Rev. B* **38**, 3287 (1988).
- [35] H. G. Winful, Delay Time and the Hartman Effect in Quantum Tunneling, *Phys. Rev. Lett.* **91**, 260401 (2003).
- [36] N. Barrett, E. E. Krasovskii, J.-M. Themlin, and V. N. Strocov, Elastic scattering effects in the electron mean free path in a graphite overlayer studied by photoelectron spectroscopy and LEED, *Phys. Rev. B* **71**, 035427 (2005).
- [37] H. Hibino, H. Kageshima, F. Maeda, M. Nagase, Y. Kobayashi, and H. Yamaguchi, Microscopic thickness determination of thin graphite films formed on SiC from quantized oscillation in reflectivity of low-energy electrons, *Phys. Rev. B* **77**, 075413 (2008).
- [38] J. Jobst, J. Kautz, D. Geelen, R. M. Tromp, and S. J. van der Molen, Nanoscale measurements of unoccupied band dispersion in few-layer graphene, *Nat. Commun.* **6**, 8926 (2015).
- [39] J. Jobst, A. J. Van Der Torren, E. E. Krasovskii, J. Balgley, C. R. Dean, R. M. Tromp, and S. J. Van Der Molen, Quantifying electronic band interactions in van der waals materials using angle-resolved reflected-electron spectroscopy, *Nat. Commun.* **7**, 13621 (2016).
- [40] H. Liu, Tunneling time through heterojunction double barrier diodes, *Superlattices and Microstructures* **3**, 379 (1987).
- [41] V. U. Nazarov, E. E. Krasovskii, and V. M. Silkin, Scattering resonances in two-dimensional crystals with application to graphene, *Phys. Rev. B* **87**, 041405 (2013).
- [42] F. Wicki, J.-N. Longchamp, T. Latychevskaia, C. Escher, and H.-W. Fink, Mapping unoccupied electronic states of freestanding graphene by angle-resolved low-energy electron transmission, *Phys. Rev. B* **94**, 075424 (2016).
- [43] E. E. Krasovskii, J. Höcker, J. Falta, and J. I. Flége, Surface resonances in electron reflection from overlayers, *Journal of Physics: Condensed Matter* **27**, 035501 (2014).
- [44] E. Economou, *Green's Functions in Quantum Physics* (Springer-Verlag, Berlin, Heidelberg, 2006).
- [45] N. Camus, E. Yakoboylu, L. Fechner, M. Klaiber, M. Laux, Y. Mi, K. Z. Hatsagortsyan, T. Pfeifer, C. H. Keitel, and R. Moshhammer, Experimental evidence for quantum tunneling time, *Phys. Rev. Lett.* **119**, 023201 (2017).
- [46] L. Torlina, F. Morales, J. Kaushal, I. Ivanov, A. Kheifets, A. Zielinski, A. Scrinzi, H. G. Muller, S. Sukiasyan, M. Ivanov, and O. Smirnova, Interpreting attoclock measurements of tunnelling times, *Nature Physics* **11**, 503 (2015).
- [47] R. O. Kuzian and E. E. Krasovskii, One-step theory of photoelectron escape time: Attosecond spectroscopy of Mg(0001), *Phys. Rev. B* **102**, 115116 (2020).
- [48] X. Oriols, F. Martín, and J. Suñé, Implications of the noncrossing property of Bohm trajectories in one-dimensional tunneling configurations, *Phys. Rev. A* **54**, 2594 (1996).
- [49] G. Grübl and K. Rheinberger, Time of arrival from Bohmian flow, *Journal of Physics A: Mathematical and General* **35**, 2907 (2002).
- [50] C. R. Leavens, Bohm trajectory approach to timing electrons, in *Time in Quantum Mechanics*, edited by J. Muga, R. S. Mayato, and Í. Egusquiza (Springer Berlin Heidelberg, Berlin, Heidelberg, 2008) pp. 129–162.
- [51] E. Krasovskii, Ab initio theory of photoemission from graphene, *Nanomaterials* **11**, 1212 (2021).
- [52] E. Krasovskii, One-step theory view on photoelectron diffraction: Application to graphene, *Nanomaterials* **12**, 4040 (2022).